

Article citation info:

Siddiqui M, Alnaser I, Alluhydan K, Assessment of a Carbon Fiber Prosthetic Running Blade for Enhanced Reliability, *Eksploracja i Niezawodność – Maintenance and Reliability* 2023; 25(4) <http://doi.org/10.17531/ein/172668>

Assessment of a Carbon Fiber Prosthetic Running Blade for Enhanced Reliability

Indexed by:



Md Irfanul Haque Siddiqui^{a,b,*}, Ibrahim Abdullah Alnaser^{a,b,c}, Khalid Alluhydan^{a,b}

^a Department of Mechanical Engineering, King Saud University, Riyadh 11451, Saudi Arabia, Saudi Arabia

^b The King Salman Center for Disability Research, Riyadh, Saudi Arabia, Saudi Arabia

^c Center of Excellence for Research in Engineering Material (CEREM), King Saud University, Riyadh 11451, Saudi Arabia

Highlights

- The durability and reliability of novel prosthetic running blades have been evaluated.
- The blade exhibits superior suitability for high-impact activities.
- The results revealed a maximum deflection of 29.60 mm that the blade can achieve.
- The outcome shows the reliability, durability, and safety of prosthetic running blades.

Abstract

This study focuses on the development of a reliable prosthetic running blade primarily composed of carbon fiber. The reliable performance of novel prosthetic running blades has been evaluated by mechanical testing and finite element numerical modeling. The experimental analysis confirmed that these blades exhibit superior suitability for high-impact activities, demonstrating reliable load-bearing capacity and effective shock absorption properties. The tensile testing exhibited a linear elastic behavior of the composite material up to a strain of 0.075 mm/mm. Further, it was found that stress concentration areas and fracture points within the blade structure. Furthermore, numerical results revealed a maximum deflection of 29.60 mm that the blade can achieve. The kinetic energy loss during impact demonstrated an 8.5% decrease in blade kinetic energy, with the highest loss occurring at $V_y = 30$ m/s. Ultimately, this research aims to enhance the reliability, durability, and safety of prosthetic running blades, empowering athletes to reach new heights in sports.

Keywords

mechanical properties, durability, prosthetic design, running blade prosthesis, materials for running blade, reliable.

This is an open access article under the CC BY license (<https://creativecommons.org/licenses/by/4.0/>)

1. Introduction

The reliability of prosthetic running blades is a critical factor in enhancing the lives of individuals with limb amputations. These innovative devices have revolutionized the field of assistive technology, enabling amputees to engage in sports and physical activities that were once deemed unattainable (13,29). The blades are engineered with lightweight materials and flexible components that absorb and release energy, propelling individuals forward with each stride. The new design reduces strain on the body and minimizes the risk of injuries, such as

stress fractures and joint damage, commonly associated with traditional prosthetic limbs or inadequate running aids. By promoting proper biomechanics and reducing impact forces, running blades contribute to improved cardiovascular fitness, enhanced muscle strength, and increased endurance(4,37). For disabled individuals, the opportunity to participate in running and athletic pursuits can be transformative.

Recently, many studies have been reported on new reliable and durable materials for prosthetic running blades, especially

(*) Corresponding author. E-mail addresses: M. Siddiqui (ORCID: 0000-0003-4289-4826) msiddiqui2.c@ksu.edu.sa, I. Alnaser (ORCID:0000-0001-6325-8410) ianaser@ksu.edu.sa, K. Alluhydan (ORCID:0000-0002-9995-8520) kalluhydan@ksu.edu.sa

carbon fiber(6,21,33). Different materials can be used in the manufacturing of prosthetic running blades include, including carbon fiber composites, thermoplastic polyethylene epoxy, and Vinylester, and some metal alloys such as high-grade aluminum alloy, steel, and titanium alloy(6,7,10,12,25,29). Carbon fiber prosthetic running blades offer several benefits and advantages over durability and reliability. It is lightweight, providing increased mobility and reduced fatigue. It is also durable and can withstand high-impact activities. This improves performance, reliability, comfort, and efficiency for athletes using prosthetic limbs during running activities. However, it is important to mention that very few research papers reported the process of manufacturing or characterization of prosthetic running blades using different materials. Abood and Faidh-Allah (1) discussed the traditional fabrication methods, which undergo rigorous testing for functionality and comfort. It investigates the performance, reliability and durability of Flex-Foot Cheetah prostheses in high-intensity activities. Specifically, two samples made of carbon and glass materials with polyester were compared. The study incorporated numerical and experimental analyses. It was found that the carbon foot sample demonstrates superior strength and reduced bending compared to the glass foot sample. Their findings contribute to the understanding of optimal materials for reliable prosthetic design in running applications. Also, Ouarhim et al. (20) explored deformations on laminated composites made of polyester matrix and glass fiber in woven and chopped strand mat forms. The number of layers affected the mechanical properties. A sports application was demonstrated through the manufacturing and characterization of leg prosthetic running blades, which showed a good agreement between experimental and numerical results. Rahman et al. (22) have reported a study on lower prosthetic limbs. It was reported that carbon fiber blades were found to be superior due to their lightness and energy retention. The study analyzed different blade designs and composite materials using finite element analysis. Ismail et al. (10) reported the different combinations of glass and carbon fibers with various polymer matrices (epoxy bakelite, casting, orthocryl, and polyester resins) can be used for a blade runner's artificial leg. They suggested that the combination of the fiber-orthocryl resin provided the best composite with the highest average tensile strength. In addition to prosthetic running

blades, some studies (11,16,35) have reported on the design of lower limbs utilizing various materials. However, the design and selection of materials for running blades have not received attention and thus very few research works have been reported.

On the other hand, numerical modeling enables a comprehensive evaluation of the prosthetic running blade's reliability, including factors such as stress distribution, strain patterns, and energy absorption(19,22,28). Moreover, numerical modeling facilitates design optimization by exploring various parameters such as materials, geometries, and structural configurations. Static behavior refers to the response of the running blade when subjected to various loads and forces while in a stationary position. The static behavior of a prosthetic running blade plays a crucial role in determining its functionality and effectiveness in providing amputees with enhanced mobility and athletic performance. Understanding the static behavior of these blades is essential for designing and optimizing their performance and reliability (3,8,35). The blade should exhibit desirable characteristics such as stiffness, flexibility, and energy storage capabilities. Stiffness is an important property of the blade, as it determines the amount of deformation or bending that occurs under load(23,24). A balance between stiffness and flexibility is necessary to ensure optimal energy return and efficient running mechanics. Zadpoor et al. (36) carried out simulations on two different types of shoes. A parametric study was undertaken to investigate the effects of masses, stiffness, damping, and gravity on the dynamics of impact. The findings indicated that impact forces increased with higher masses and touchdown velocities. The influence of damping coefficients on the force was found to be greater than that of stiffness. Further, it is reported (13) that the shape and geometry of the blade also contribute to its static behavior. The curvature and thickness of the blade affect its stiffness and flexibility. These factors need to be carefully considered to ensure that the blade provides the desired level of support and responsiveness. In addition to this, explicit dynamic analysis is a computational method used to simulate the dynamic response of prosthetic running blades under various loading conditions (34). This analysis technique is crucial for understanding the behavior of the blade during high-impact activities such as running and jumping. The blade can be modeled with realistic material behavior, considering its

nonlinear elasticity, damping, and energy dissipation characteristics. This enables the simulation to capture the dynamic response of the blade more accurately and provide insights into its performance under different loading scenarios. Shu-Sheng Bi et al. (5) presented a novel model for studying the impact dynamics of compliant-legged robots. The effectiveness of the model was validated using the finite element program LS-DYNA, considering velocity and energy aspects. It was reported that the post-impact vertical velocity of the robot decreased with increasing incident angles and a discussion was made on the kinetic energy of the blade after impact. However, a practical approach is still due to evaluate the impact of running blades using practical design and carbon fiber. In a separate study, Balaramakrishnan et al. (2) employed a numerical method to pre-determine several biomechanical parameters of a prosthetic foot's stance phase. These parameters included roll-over characteristics, the center of pressure trajectory, ankle flexion moment arm, and ankle range of motion, all of which assisted in the foot's design process. Some other literature (9,14,27) (15,26,31) has been reported on numerical analysis of socket design, artificial knee, leg etc. Nevertheless, there remains a significant research gap in the field concerning the fabrication techniques of prosthetic running blades and their subsequent evaluation in terms of performance, durability and reliability through mechanical testing and finite element analysis. Addressing this gap is crucial to enhance our understanding of the design and functionality of prosthetic running blades.

In the current study, a laboratory-based development was undertaken to create a prosthetic running blade utilizing carbon fiber as the primary material. The blade's construction involved the use of laminated carbon fiber materials. Following fabrication, mechanical testing was conducted to evaluate the blade's performance and functionality. Furthermore, a finite element simulation was employed to analyze the behavior of the running blade. Initially, a static analysis was performed to examine how the blade responded to varying loads and forces. In addition, an explicit analysis was carried out to study the blade's motion subsequent to an impact and to quantify the dissipation of energy during the impact event.

2. Materials and Methods

2.1. Experimental Setup

The use of carbon fiber layers in the manufacturing process has played a pivotal role in creating lightweight and durable running blades that mimic the biomechanics of natural limbs. The dimensions details of running blade have been shown in Figure 1(a). The prosthetic running blade has been made in laboratory using carbon fiber sheets.

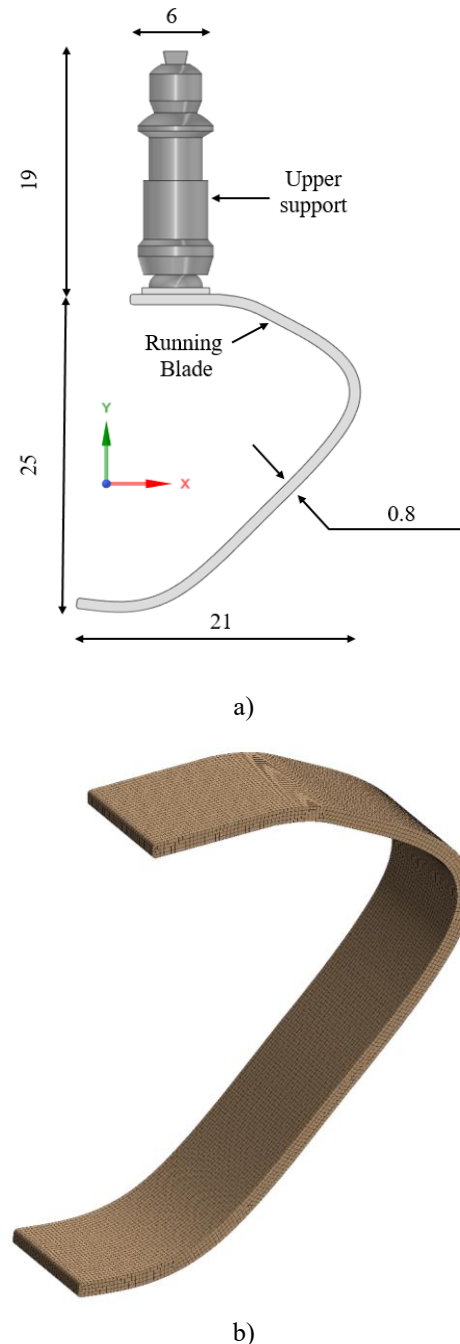


Figure 1. Schematics of prosthetic running blades (a) dimensions (b) discretized domain for simulation (dimensions in cm).

Firstly, a wooden mold was made based on dimensions. The upper surface of mold was laminated with aluminum in order to get a smooth surface. The carbon fiber sheets were shaped and layered over the mold to form a running blade with precise attention to structural integrity. Further, the carbon fiber blade was subjected to a curing process to optimize strength and stiffness. The process of running blade fabrication has been shown in Figure 2. To test its mechanical behavior, the running blade interface was tailored to the fixed in bending test machine. The alignment of the running blade was checked to ensure optimal biomechanics, energy return, and proper weight distribution during running. Further, to perform the tensile test,

dog-bone-shaped samples with dimensions of (50 mm x 12.5 mm x 6.25 mm) were prepared. For the compression test, cylindrical samples with dimensions of 25.4 mm and a height of 50 mm were created. These samples were placed vertically in the compression testing machine, and axial compression was applied at a specified rate until either failure occurred. In the flexural test, rectangular samples with dimensions of 127 mm in length, 12.7 mm in width, and a thickness of 3.2 mm were fabricated. These samples were positioned on two supports. A vertical load was applied at the center of the samples until either failure was achieved.

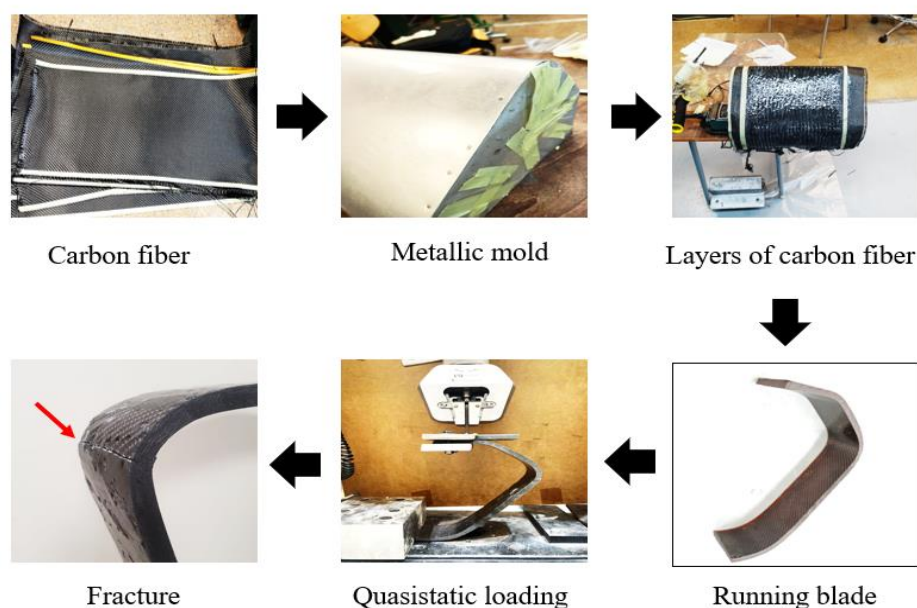


Figure 2. Sequence of steps involved in the fabrication of running blades.

2.2. Numerical Modeling

In this work, we have used carbon fiber epoxy composite material for running blade simulation. We have used a similar design of a commercially available running blade by Levitate Technology ApS (Roskilde), Denmark. The design of the running blade has been studied very carefully and transformed into a three-dimensional CAD model. The geometry has been made on SpaceClaim software (Ansys Inc.). Further, meshing and structural analysis has been carried out on Ansys Mechanical software. In this numerical work, the force has been applied on the top of the assembly of the running blade. The force (1100 N) was applied vertically to the running blades for static behavior analysis. The design of the running blade is inspired by the commercially available running blade. The

dimensions and meshing details of the running blade are presented in Figure 1(a). The elements mesh has been shown in Fig. 1(b). Lastly, we have carried out explicit finite element numerical modeling of prosthetic running blades. The material properties have been provided in Table 1. The prosthetic running blade CAD diagram is shown in the figure with the all-dimension details. The leg is constructed of carbon fiber with high restitution. In this numerical model, we have chosen a specific number of elements by grid independence test. The details of mesh size and the number of elements have been illustrated in Table 2. We took total deformation at the midplane of the running blade as the criterion to judge the suitability of the number of elements. From the results of total deformation, we concluded that mesh size 66,071 is most suitable for

producing acceptable results

Table 1. Material properties.(20,19,30,32).

No	Property	Materials
		Carbon-Fiber
1	Modulus of Elasticity (GPa)	230
2	Poisson's Ratio	0.2
3	Yield Strength (MPa)	2500
4	Tensile strength Ultimate (MPa)	3590
5	Comp. strength (MPa)	-
6	Density (kg/m ³)	1750
7	Melting Point (°C)	3652

Table 2. Mesh size and total deformation.

S. No.	No. of Nodes	No. of Elements	Total deformation (mm)
1	116,058	30,050	26.37
2	206,502	66,071	29.48
3	360,558	91,007	29.63

3. Description of Impact Modeling

Figure 1 displays the prosthetic running blade under analysis, comprising a running blade and a compliant support fixed to the surface below. The system is simplified as a rigid body denoted as B, along with a flexible leg referred to as L, which consists of a thin leaf with a rectangular shape. The impact occurs when the running blade is dropped from a specified height. The objective is to forecast the overall motion of the running blade following the impact and assess the energy loss during this process. The kinematic and kinetic modeling of the running blade is derived from the work of Bi et al. (5).

3.1. Kinematic relationship

To characterize the movements of the running blade within the global frame of reference XOY, we can represent the position vector of any arbitrary point as follows:

$$r_c = r_j + A_L u_p^L \quad (1)$$

where the position vectors r_j , u_p^L and the transformation matrix A_L

It is important to highlight that the elastic deformation vector of point D can be expressed as follows:

$$d_f = [d_1 \quad d_2]^T \quad (2)$$

the axis and transverse elastic displacements of point D are represented by u_1 and u_2 , respectively.

$$d_2(x, t) = \sum_{i=1}^n \phi_i(x) q_i(t) \quad (3)$$

In this context, the variable n represents the chosen number of vibrational modes, while $\phi_i(x)$ represents the selected mode

shape of the running blade.

$$\phi_i(x) = \cosh\left(\frac{\lambda_i x}{l}\right) - \cos\left(\frac{\lambda_i x}{l}\right) - \gamma_i \left[\sinh\left(\frac{\lambda_i x}{l}\right) - \sin\left(\frac{\lambda_i x}{l}\right) \right] \quad (4)$$

with

$$\gamma_i = \frac{\cosh \lambda_i + \cos \lambda_i}{\sinh \lambda_i + \sin \lambda_i}$$

where λ_i is the consecutive root of the transcendental equation.

By taking the derivative of equation (1) with respect to time, we can determine the velocity vector of any arbitrary point on running blade.

$$\dot{r}_c = \dot{r}_j + \dot{A}_L u_p^L + A_L \dot{u}_p^L \quad (5)$$

3.2. Kinetic energy.

Using the kinematic relationship mentioned earlier, we can express the kinetic energy of the running blade as follows:

$$T_L = \frac{1}{2} \rho_L \int_0^l \dot{r}_c^T \cdot \dot{r}_c \, dx = \frac{1}{2} \dot{q}_L^T M_L \dot{q}_L \quad (6)$$

Here, $\rho_L = m_L/l$ represent the mass of the leg per unit of length and \dot{q}_L the generalized speed vector.

We can represent the mass matrix of the robot as follows:

$$M = \begin{bmatrix} M_B & 0 \\ 0 & M_L \end{bmatrix} \quad (7)$$

3.3 Forces

An approximate expression for the elastic strain energy stored in the running blade can be formulated as follows:

$$U_L = \frac{1}{2} \int_0^l E_1 I \left(\frac{\partial^2 u_2(x,t)}{\partial x^2} \right)^2 \, dx = \frac{1}{2} q_L^T K_{ff} q_L \quad (8)$$

By substituting equations (3) and (4) into equation (11), the stiffness matrix of the running blade K_{ff} can be obtained.

The external forces exerted on the running blade comprise the weight and the contact force F_S applied at the contact point T. The weight is comprised of $m_L g$ and $m_B g$, representing the weights acting at the center of L and D, respectively. The vector representation of F_S can be expressed as follows:

$$F_S = [F_t \quad F_n]^T \quad (9)$$

Here, F_n and F_t represent the normal and tangential forces, respectively, exerted by the surface at the contact point.

3.4 Energy loss analysis

The energy lost by the prosthetic running blade during the impact can be formulated as follows.

$$E_r = \Delta E_{tD} + \Delta E_{tL} \quad (10)$$

Where ΔE_{tD} and ΔE_{tL} represent the changes in total energy of the body and leg, respectively, during the impact.

$$\Delta E_{tD} = \Delta E_{kD} + \Delta E_{gD} \quad (11)$$

$$\Delta E_{tL} = \Delta E_{kL} + \Delta E_{gL} + \Delta E_{eL} \quad (12)$$

Where ΔE_{kD} , ΔE_{kL} , ΔE_{gD} and ΔE_{gL} represent the variations in kinetic energy and gravitational potential energy of D and L, respectively. ΔE_{eL} denotes the change in elastic strain energy of the running blade during the impact.

Let η_r represent the energy loss ratio of the robot, which can be expressed as:

$$\eta_r = \frac{E_t}{E_t} \quad (13)$$

where E_t is the total energy

$$E_t = E_{ki} + E_{pi} \quad (14)$$

where E_{ki} and E_{pi} denote the initial kinetic and potential energy, respectively.

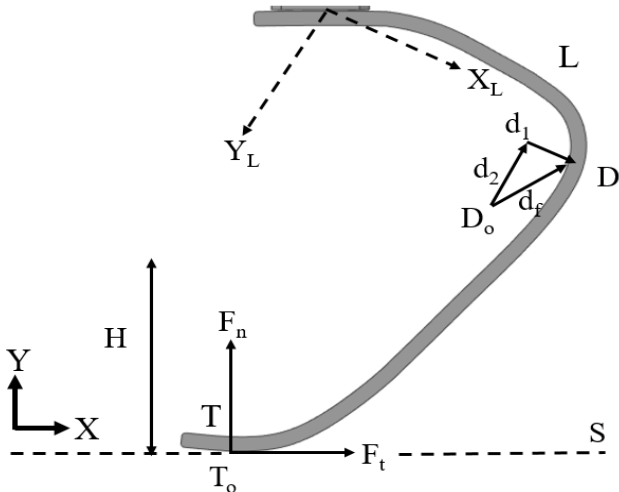


Figure 3. Schematic diagram depicts the force balance on running blade.

4. Results and Discussion

4.1. Experimental Results

The quasi-static compressive test has been carried out on prosthetic running blade as shown in Figure 4. Further, Figure 5 shows the plot of experimental results of quasi-static compressive displacement test of prosthetic running blade made from carbon fiber. The quasi-static compressive extension has been used to evaluate the behavior of carbon fiber under compressive forces applied at a slow and controlled rate. In this testing method, running blade was subjected to an increasing compressive load, and the resulting deformation was measured. In our experiment, the loading rate was slow enough to assume

equilibrium at each step of the loading process. This helped carbon fiber blade to have sufficient time to adjust to the applied load and redistribute stresses before further loading occurred. The obtained data from quasi-static compressive extension tests has been shown as graphical plot in Figure 5. It can be observed that deformation started as the load was increased. The elastic deformation was recorded till 1100 N that contributed in 23 mm deformation. The yielding point occurs at maximum force 1120 N and plastic deformation continued till 57 mm. The further compressive extension subjected to fracture of running blade at 986 N. The fractured running blade has been shown as shown in the inset in figure 5. The indicates that the blade had enough reliable load-bearing capacity for sprinting and running activity.



Figure 4. Visuals of sample fixed for quasi-static bending test.

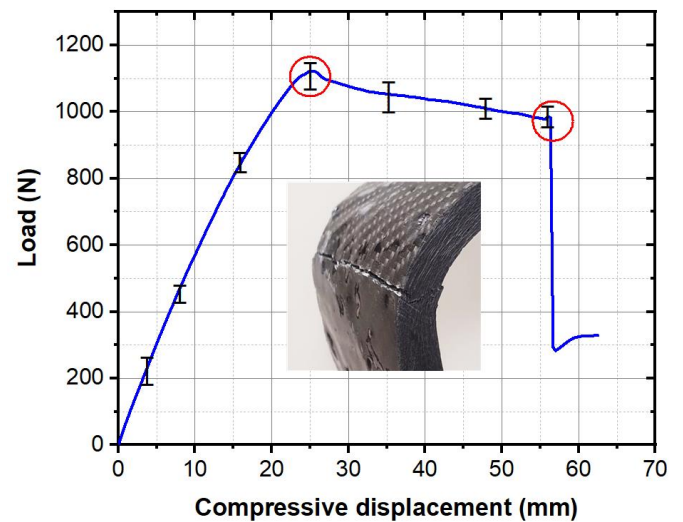


Figure 5. Experimental results of quasi-static compressive displacement test of prosthetic running blade made from carbon fiber.

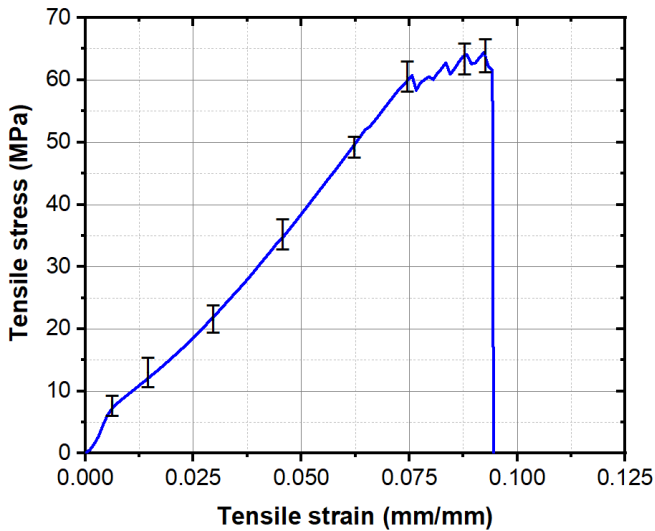


Figure 6. Stress-strain plot for tensile test of carbon fiber specimen.

The stress-strain diagram shown in Figure 6 depicts the relationship between the applied stress and the resulting strain in the carbon fiber specimen. As the specimen is subjected to increasing tensile strain, the stress experienced by the material increases. Looking at the data, we observe that as the tensile strain increases, the tensile stress also increases. Initially, the trend seems more linear. However, beyond this point, the stress-strain trend remains constant up to 0.075 mm/mm. This indicates that the carbon fiber composite exhibits a linear elastic behavior within the tested range. Initially, the relationship between stress and strain appears to be approximately linear, indicating the material's ability to undergo deformation without permanent damage. As the strain continues to increase, the stress-strain curve deviates from linearity, suggesting the material may undergo some plastic deformation at 60 MPa. This deviation could be attributed to the composite material's structure and the interactions between the carbon fibers and the epoxy material which was used for the bonding of the layers. Beyond 60 MPa stress, it appears that the fracture in the specimen was significantly increased and it collapsed reaching 65 MPa.

Figure 7 represents the experimental results of the compressive test of the carbon fiber specimen. In the initial region of the plot, the compressive extension was 0 mm, and the load values were relatively low. This indicated that there was no significant resistance to compression initially, and the specimen underwent elastic deformation. Additionally, the load values in this region were relatively consistent and low, suggesting that

the material was in its linear elastic range. As the load increased, compressive displacement also increased linearly. The specimen exhibited elastic behavior, meaning it returned to its original shape after the load was removed (around 8000 N). The slope of the linear portion in the plot represented the material's stiffness or Young's modulus in compression. Furthermore, beyond 10,000 N, the plot transitioned from the linear elastic region to a non-linear region. It indicated that the material started to undergo plastic deformation, where it retained a certain amount of deformation after the load was removed. Moreover, in the non-linear region, the compressive displacement continued to increase, but the rate of load increase slowed down. It indicated that the material was undergoing plastic deformation and started to experience stress redistribution and microstructural changes. The plot reached a peak load of 21,000 N, which represented the maximum load-carrying capacity (visually 1.6 mm compression). At this point, the material had started to experience localized deformations, such as microcracks or fiber/matrix damage. Also, the load started to decrease, indicating material failure or fracture.

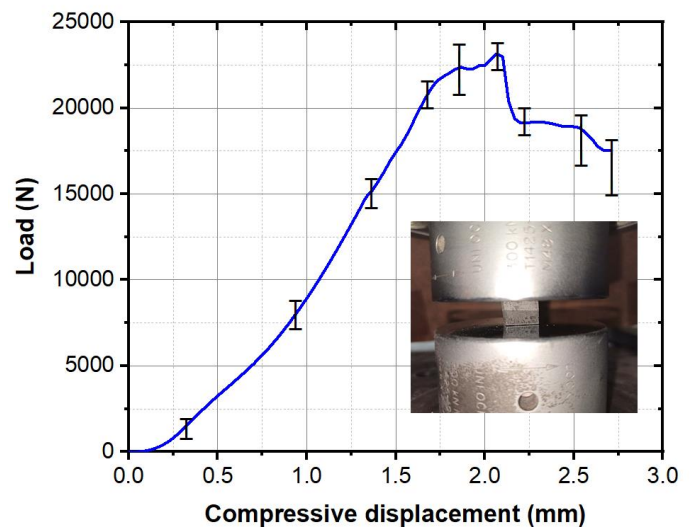


Figure 7. Compressive test plot for the running blade specimen.

The plot of the flexure load test of the carbon fiber epoxy composite has been shown in Figure 8. It is noted that the flexure load increases with the extension, which is expected in a flexure test. As the specimen is subjected to increasing extension, it experiences higher stress, leading to an increase in load. Initially, the relationship between extension and flexure load appears to be linear at very less load. Beyond this the curve starts to deviate from linearity, indicating a nonlinear behavior

of the material. Further, the flexure load shows a gradual increase up to an extension of approximately 0.4 mm, after which the rate of increase becomes steeper.

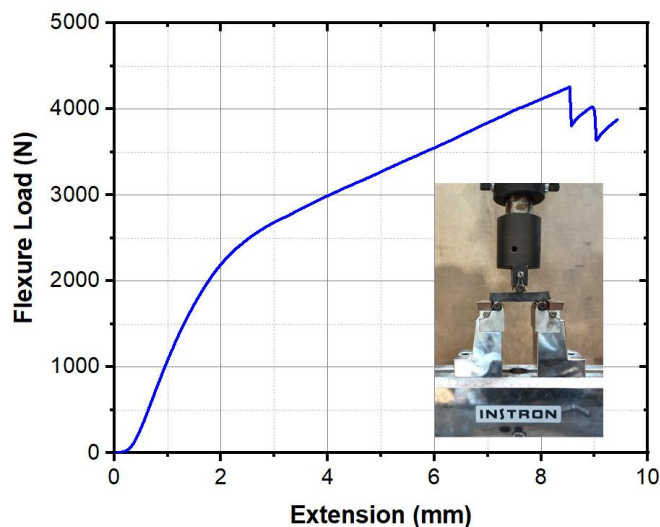


Figure 8. Flexure test plot for carbon fiber specimen.

This indicates that the material initially behaves elastically, followed by yielding or plastic deformation. Beyond an extension of approximately 2.8 mm, the flexure load levels off, signifying that the material has reached its maximum load-bearing capacity. This plateau phase implies substantial plastic deformation or fracture is occurring. The plot shows some scatter in the data points, which may be due to experimental variability or fluctuations in the material properties. The maximum flexure load achieved in the test is approximately 4270 N, occurring at an extension of around 9.4 mm. It's worth noting that there seems to be a sudden drop in the flexure load data after an extension of 8.0 mm, followed by a partial recovery. This sudden drop could indicate a failure or fracture event in the specimen. Figure 8 depicts the specimen of carbon fiber epoxy composite exhibits a combination of elastic and plastic deformation behavior. It initially behaves elastically, then undergoes plastic deformation until reaching its maximum load capacity, potentially leading to fracture.

4.2 Finite Element Analysis

Furthermore, we conducted a finite element simulation to analyze the static behavior of the blade. Figure 9 illustrates an equivalent von Mises stress under a static load of 1100 N on running blades fabricated from carbon fiber material. The von Mises stress presented here serves as an indicator for assessing

the potential yielding or failure of the running blade under combined loading conditions, as it is derived from the principle of distortion energy theory. Moreover, it is assumed that failure is more prone to occur due to shear stresses rather than normal stress. It was noted that the maximum value of equivalent von Mises stress was 471 MPa. It is important to note that the maximum stress values should not exceed during sports activities, as the applied static load surpasses these values. Since the load on the running blade originates from uniaxial loading, which provides a single scalar value of stress, we observe stress concentration at the bending position in all cases, as depicted in Figure 9. The experimental results further confirm that fracture occurs at the bend position.

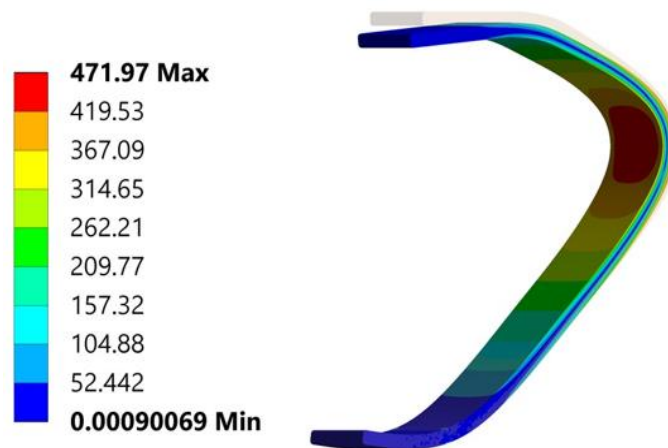


Figure 9. Equivalent von Mises stress (MPa) under 1100 N static load.

To get comprehensive information of fracture, we generated a plot of total deformation. Figure 10 shows the total deformation by the blade subjected to external static loading. The total deformation parameter affects the energy return and assists amputees in engaging in other athletic movements. It was observed that the total deformation in a running blade was influenced by material properties. Moreover, it is also influenced by various factors, including the design features, and the applied loads. It can be noted that carbon fiber have maximum deflection 29.60 mm. It is interesting to note that total deformation appears at the top of the running blade due to maximum deflection shown by top surface. Furthermore, deflection due to load can be also observed at upper half part of running blade. It is important to have the deformation under within a desirable range to maximize performance and comfort while minimizing the risk of damage or failure.

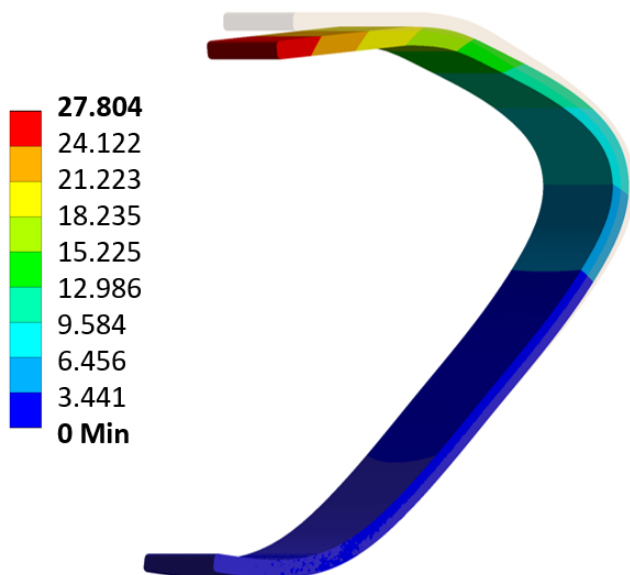


Figure 10. Total deformation under static loading condition for Carbon Fiber. (Deformation in mm).

This plot is helpful to visualize the total deformation at maximum static load 1100 N applied by the user thus, it can help in optimizing the design and material selection to achieve the desired deformation characteristics. Figure 11 shows the stress concentration and fracture during static loading condition.

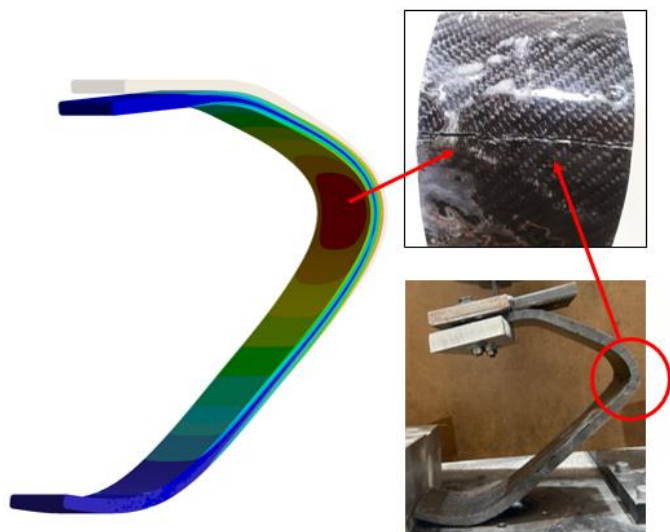


Figure 11. Stress concentration and fracture occurrence shown in static loading condition.

It should be also noted that excessive deformation may lead to reduced energy return, instability, or discomfort. In contrast, insufficient deformation can result in limited shock absorption and compromised running performance. To achieve this, a balance must be made to provide an optimal level of deformation that meets the specific requirements of the user. This optimization could be done by iterative design that would be based on different factors such as their weight, running style,

and activity level. In a prosthetic running blade, identifying stress concentration and fracture points through finite element analysis is significant as it helps us pinpoint areas vulnerable to structural failure. Addressing these points can lead to improved blade design, durability, and ultimately, enhanced performance and safety for amputees.

Figure 12 represents the variation of the contact deflection during the impact. The graph plots between reaction force and velocity in vertical downward direction ($V_y = 1 \text{ m/s}$). It is evident that increases from 0 to maximum in the first half phase and declines to zero in the latter half phase. This means that the elastic compression and restitution phases are experienced successively by the running blade. When a prosthetic running blade makes an impact with a rigid surface, the force reaction versus time can be understood by considering the mechanics of the interaction. As the prosthetic running blade comes into contact with the rigid surface, the force begins to build up gradually. Initially, the force is relatively low as the blade starts to compress and absorb the impact. As the blade continues to contact the rigid surface, it undergoes compression due to the applied force. The force reaction increases as the blade compresses, reaching its peak when the compression is maximum. The peak force occurs when the prosthetic running blade is fully compressed and has reached its maximum deformation. This peak force represents the maximum resistance encountered during the impact. After reaching the peak force, the prosthetic blade starts to release the stored energy, causing a recoil or rebound effect. This recoil force is lower than the peak force and helps to propel the user forward. As the prosthetic blade continues to recoil and return to its original shape, the force decreases gradually. Eventually, the prosthetic blade completely separates from the rigid surface, and the force drops to zero. This marks the end of the impact phase. It's important to note that the specific force reaction versus time curve can vary depending on factors such as the design and properties of the prosthetic running blade, the rigidity of the surface, and the individual's running technique. Prosthetic blades are engineered to provide a balance between shock absorption, energy storage, and efficient running mechanics to minimize the impact forces experienced by the user. In a prosthetic running blade, the expected impact dynamic involves the blade compressing upon contact with the ground,

storing potential energy in its flexible structure. This energy is then released, propelling the amputee forward, mimicking the natural spring-like motion of a human foot.

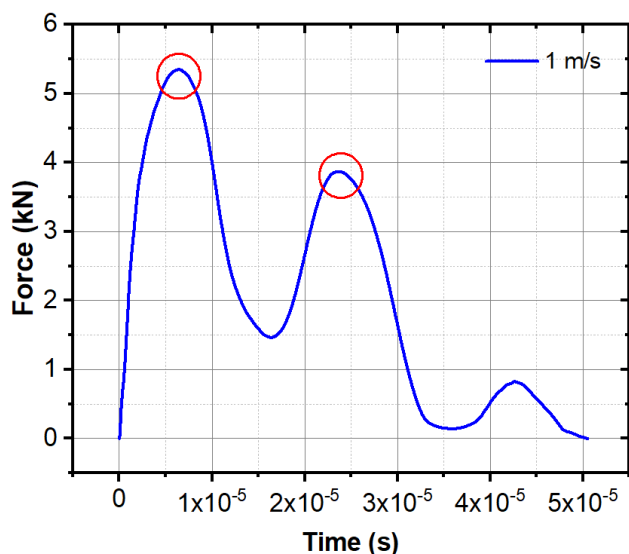


Figure 12. Plot of force vs time during impact of running blade on surface ($v = 1\text{ m/s}$).

Further, Fig. 13 shows the force vs time plot for prosthetic running blade for different velocities (V_y).

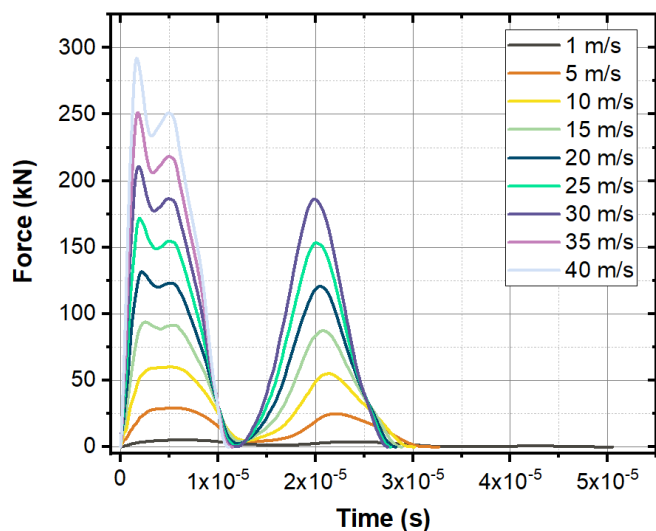


Figure 13. Plot of force vs time during impact of running blade on surface at different impact velocities (V_y).

The plot compares the forces at the contact point at different vertical V_y velocities. The plot for $V_I=1\text{ m/s}$ (shown in Figure 9) illustrates the load at fraction of time (up to 6×10^{-6} seconds). It can be observed here that force reaction is fluctuating with respect to time. The maximum force reaction during initial impact was 5.3 kN at 0.8×10^{-6} second for vertical downward velocity $V_I=1\text{ m/s}$. Further, force reaction decreases with respect to time and a significant reduction has been observed after 3×10^{-6}

seconds. Subsequently, we compared the force reaction at different vertical velocity conditions $V_y = 1, 5, 10, 15, 20, 25, 30, 35$ and 40 m/s , as shown in Fig. 13. It can be noted that force reaction increases with respect to velocity in y direction. The force reaction reaches up to 133 kN at $V_y = -20\text{ m/s}$. Secondly, reaction force decreases for all case of V_y at time 1.2×10^{-6} second and increase to another peak 2.1×10^{-6} second. Further, we observe that reaction forces decrease to insignificant values near 3×10^{-6} second. One of interesting finding is that higher V_y values have two peaks before 1.2×10^{-6} second time.

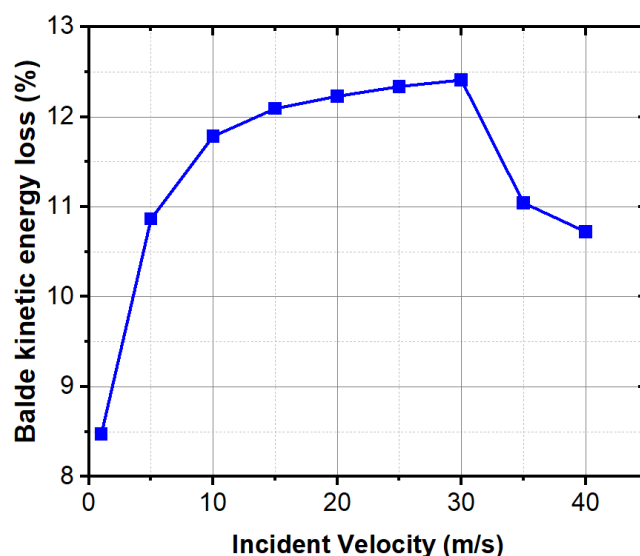


Figure 14. Plot of blade kinetic energy vs incident velocity.

Figure 14 shows the percentage blade kinetic energy loss with respect to incident velocity (V_y). When a prosthetic running blade makes an impact with a rigid surface, there is a loss of kinetic energy due to various factors. Upon impact, the prosthetic running blade undergoes compression and deformation as it absorbs the energy from the collision. This deformation represents a loss of kinetic energy, as some of the initial energy is transformed into potential energy stored within the blade. The plot in Figure 14 signify the losses occurs during impact. It can be noted here that the percentage of blade kinetic energy loss is 8.5 percent. Further, percentage loss increases with respect to velocity until $V_y=-30\text{ m/s}$. Afterward, percentage blade kinetic energy loss decreases when velocity is significantly higher such as $V_y=-35$ and -40 m/s . The maximum loss occurs at $V_y=-30\text{ m/s}$ which corresponds to 12.4% blade kinetic energy. Also, blade kinetic energy loss significantly rises at lower incident velocity ($V_y = -1$ to -10 m/s). However, the change in blade kinetic energy loss is less than 1% for $V_y = -10$

to -30 m/s. Further, change in loss is just 2% when velocity is increased from $V_y = -30$ to -40 m/s. It is worth noting that prosthetic running blades are designed to reduce the blade kinetic energy.

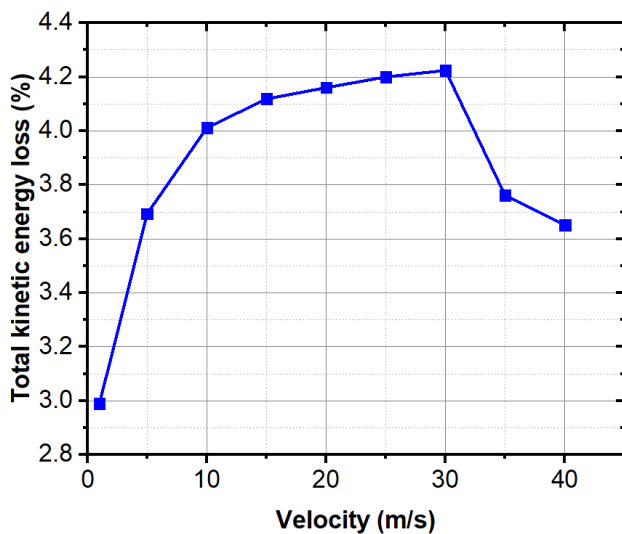


Figure 15. Total kinetic energy loss vs incident velocity.

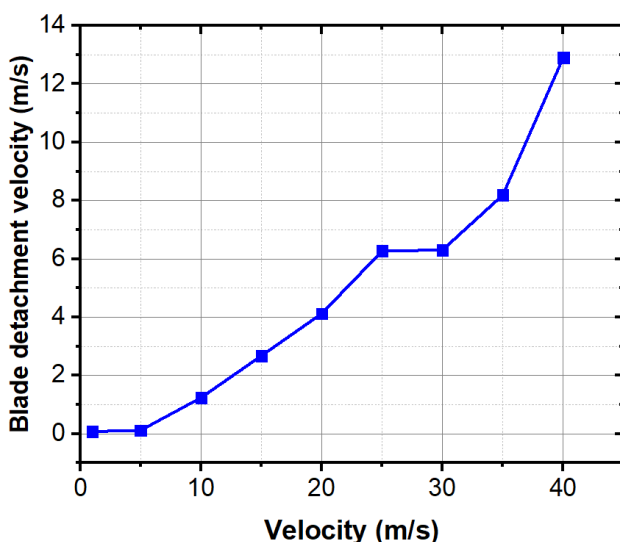


Figure 16. Plot of blade detachment velocity with respect to incident velocity (V_y).

In order to make it simpler, we plotted the total kinetic energy loss during the different incident velocities, as shown in Figure 15. It is observed here that loss in total kinetic energy is 3% at $V_y = -1$ m/s. Further loss increases with respect to incident velocity up to $V_y = -30$ m/s. The total kinetic energy loss increases rapidly at lower velocities ($V_y = -1$ to -10 m/s) where total change in loss corresponds to 0.7%. In contrast to this, the change in total loss corresponds to less than 0.2% for higher velocities ($V_y = -10$ m/s to -30 m/s). Energy losses within the prosthetic running blade can significantly impact its overall

performance. These losses may reduce the blade's efficiency in converting impact energy into forward motion, potentially leading to decreased running speed, increased fatigue, and less comfort for the user.

Furthermore, the detachment velocity of a prosthetic running blade is shown in Figure 16. It can be noted that detachment velocity is affected by the user's running activity (velocity, V_y). It is noted from the graph that the detachment velocity of the running blade increased with the increment in incident velocity (V_y). It is well known that high-impact activities such as sprinting or jumping exert greater force on the blade, which can increase the likelihood of detachment if the attachment is not secure enough. This plot could be used to design the attachments for the running blades. To enhance user safety during high-impact activities, consider implementing more robust locking systems and integrating shock-absorbing components into the attachment mechanism. Regular maintenance and user feedback can help ensure these improvements are effective and reliable.

5. Conclusions

The experimental and finite element analysis results provided valuable insights into the performance, reliability and durability of prosthetic running blades made from carbon fiber. The experimental analysis confirmed the carbon fiber prosthetic running blade's suitability for high-impact activities, demonstrating sufficiently reliable during load-bearing capacity and shock absorption properties. The conclusions from current work has been summarized as follows:

- The quasi-static compressive test revealed that the carbon fiber blade exhibited elastic deformation up to a maximum force of 1120 N, followed by plastic deformation until fracture occurred at 986 N. The tensile test showed a linear elastic behavior of the carbon fiber composite up to a strain of 0.075 mm/mm, beyond which it exhibited plastic deformation. The compressive test demonstrated that the material underwent elastic deformation initially and then transitioned to non-linear behavior and reaching its maximum load-carrying capacity at 21,000 N

- Finite element analysis provided valuable insights into stress concentration areas and fracture points. The von-Mises stress analysis showed stress concentration at the bending position, indicating potential failure points. The total deformation analysis indicated that carbon fiber blades could achieve maximum deflection of 29.60 mm, primarily occurring at the top surface.
- Force-time plots at different impact velocities revealed variations in force reactions, particularly at higher velocities, where two peaks were observed before 1.2×10^{-6} seconds, indicating complex energy transfer dynamics. The force-time plot at different velocities highlighted the increase in force reaction with velocity in the vertical direction, reaching a maximum of 133 kN at $V_y = -20$ m/s. The analysis of kinetic energy loss during impact revealed an 8.5% loss in blade kinetic energy, with the maximum loss occurring at $V_y = -30$ m/s. The total kinetic energy loss during impact increased rapidly at lower velocities ($V_y = -1$ to -10 m/s) and remained relatively stable at higher velocities ($V_y = -10$ to -30 m/s).
- The detachment velocity of the blade increased with incident velocity, emphasizing the importance of secure attachments for high-impact activities. The detachment velocity of the running blade was influenced by the incident velocity (V_y), highlighting the need for secure attachments based on the user's running activity.
- Overall, these findings contribute to a better understanding of the performance, reliability and durability of prosthetic running blades made from carbon fiber and provide insights for optimizing their design, material selection, and attachment mechanisms to enhance performance, comfort, and durability while minimizing the risk of failure.

Funding

This research was funded by the King Salman Center For Disability Research through Research Group no KSRG-2022-041.

Acknowledgments

The authors extend their appreciation to the King Salman Center For Disability Research for funding this work through Research Group no KSRG-2022-041.

References

1. Abood SH, Faidh-Allah MH. Analysis of Prosthetic Running Blade of Limb Using Different Composite Materials. *Journal of Engineering*. 2019;25(12):15–25. <https://doi.org/10.31026/j.eng.2019.12.02>
2. Balaramakrishnan TM, Natarajan S, Sujatha S. Biomechanical design framework for prosthetic feet: Experimentally validated non-linear finite element procedure. *Med Eng Phys*. 2021;92. <https://doi.org/10.1016/j.medengphy.2021.04.006>
3. Barnett CT, De Asha AR, Skervin TK, Buckley JG, Foster RJ. Spring-mass behavioural adaptations to acute changes in prosthetic blade stiffness during submaximal running in unilateral transtibial prosthesis users. *Gait Posture*. 2022;98. <https://doi.org/10.1016/j.gaitpost.2022.09.008>
4. Bellmann M, Schmalz T, Ludwigs E, Blumentritt S. Immediate Effects of a New Microprocessor-Controlled Prosthetic Knee Joint: A Comparative Biomechanical Evaluation. *Arch Phys Med Rehabil*. 2012 Mar 1;93(3):541–9. <https://doi.org/10.1016/j.apmr.2011.10.017>
5. Bi SS, Zhou XD, Marghitu DB. Impact modelling and analysis of the compliant legged robots. *Proceedings of the Institution of Mechanical Engineers, Part K: Journal of Multi-body Dynamics*. 2012;226(2):85–94. <https://doi.org/10.1177/1464419312441451>
6. Che Me R, Ibrahim R, Md. Tahir P. Natural based biocomposite material for prosthetic socket fabrication. *ALAM CIPTA, International Journal on Sustainable Tropical Design Research & Practice*. 2012;5(1).

7. Coombes AGA, Maccoughlan J. Development and testing of thermoplastic structural components for modular prostheses. *Prosthet Orthot Int.* 1988;12(1):19–40. <https://doi.org/10.3109/03093648809079387>
8. Groothuis A, Houdijk H. The Effect of Prosthetic Alignment on Prosthetic and Total Leg Stiffness While Running With Simulated Running-Specific Prostheses. *Front Sports Act Living.* 2019;1. <https://doi.org/10.3389/fspor.2019.00016> <https://doi.org/10.3389/fspor.2019.00016>
9. Hameed MI, Abdul A, Ali H. Finite Element Design and Manufacturing of a Woven Carbon Fiber Prosthetic Foot. *Association of Arab Universities Journal of Engineering Sciences.* 2022;29(2).
10. Ismail R, Paras Utami D, Arid Irfai M, Jamari J, Bayuseno AP. Mechanical properties of Carbon-matrix composites for a blade runner's artificial leg. *Cogent Eng.* 2021;8(1). <https://doi.org/10.1080/23311916.2021.1923382>
11. Kathrotiya D, Yusuf A, Bhagchandani RK, Gupta S. A Study for the development of prosthetic foot by additive manufacturing. *Journal of the Brazilian Society of Mechanical Sciences and Engineering.* 2023;45(3). <https://doi.org/10.1007/s40430-023-04107-y>
12. Kitila LG, Wolla DW. Fabrication, characterization, and simulation of hybrid flax-sisal fiber reinforced epoxy composite for prosthetic limb socket application. *J Compos Mater.* 2022;56(10). <https://doi.org/10.1177/00219983221080890>
13. Lee WCC, Zhang M, Boone DA, Contoyannis B. Finite-element analysis to determine effect of monolimb flexibility on structural strength and interaction between residual limb and prosthetic socket. *J Rehabil Res Dev.* 2004 Nov;41(6 A):775–86. <https://doi.org/10.1682/JRRD.2004.01.0003>
14. Maitland ME, Allyn KJ, Ficanha EM, Colvin JM, Wernke MM. The Effect of Single and Multiple Split-Toe Designs on Cross-Slope Adaptability of Prosthetic Feet: A Finite Element Simulation Study. *Journal of Prosthetics and Orthotics.* 2023;35(1). <https://doi.org/10.1097/JPO.0000000000000427>
15. Maitland ME, Allyn KJ, Ficanha EM, Colvin JM, Wernke MM. Finite Element Simulation of Frontal Plane Adaptation Using Full-Foot, Split-Toe, and Cam-Linkage Designs in Prosthetic Feet. *Journal of Prosthetics and Orthotics.* 2022;34(1). <https://doi.org/10.1097/JPO.0000000000000363>
16. Manufacturing of personalized prosthetic leg using solid modeling and 3d printing. *Letters in Applied NanoBioScience.* 2020;9(1). <https://doi.org/10.33263/LIANBS91.892896>
17. Meziani Y, Morère Y, Hadj-Abdelkader A, Benmansour M, Bourhis G. Towards adaptive and finer rehabilitation assessment: A learning framework for kinematic evaluation of upper limb rehabilitation on an Armeo Spring exoskeleton. *Control Eng Pract.* 2021 Jun 1;111. <https://doi.org/10.1016/j.conengprac.2021.104804>
18. Millstein S, Bain D, Hunter GA. A review of employment patterns of industrial amputees—factors influencing rehabilitation. *Prosthet Orthot Int.* 1985;9(2):69–78. <https://doi.org/10.3109/03093648509164708>
19. Noroozi S, Sewell P, Rahman AGA, Vinney J, Chao OZ, Dyer B. Modal analysis of composite prosthetic energy-storing-and-returning feet: An initial investigation. *Proc Inst Mech Eng P J Sport Eng Technol.* 2013;227(1):39–48. <https://doi.org/10.1177/1754337112439274>
20. Ouarhim W, Ait-Dahi M, Bensalah MO, el Achaby M, Rodrigue D, Bouhfid R, et al. Characterization and numerical simulation of laminated glass fiber–polyester composites for a prosthetic running blade. *Journal of Reinforced Plastics and Composites.* 2021;40(3–4):118–33. <https://doi.org/10.1177/0731684420949662>
21. Phillips SL, Craelius W. Material properties of selected prosthetic laminates. *Journal of Prosthetics and Orthotics.* 2005 Jan;17(1):27–34. <https://doi.org/10.1097/00008526-200501000-00007>
22. Rahman M, Bennett T, Glisson D, Beckley D, Khan J. Finite element analysis of prosthetic running blades using different composite materials to optimize performance. *ASME International Mechanical Engineering Congress and Exposition, Proceedings (IMECE).* 2014;10(1):1–14. <https://doi.org/10.1115/IMECE2014-37293>
23. Richard V, Lamberto G, Lu TW, Cappozzo A, Dumas R. Knee Kinematics Estimation Using Multi-Body Optimisation Embedding a Knee Joint Stiffness Matrix: A Feasibility Study. *PLoS One.* 2016 Jun 1;11(6). <https://doi.org/10.1371/journal.pone.0157010>
24. Sancisi N, Parenti-Castelli V. A sequentially-defined stiffness model of the knee. *Mech Mach Theory.* 2011 Dec;46(12):1920–8. <https://doi.org/10.1016/j.mechmachtheory.2011.07.006>
25. Schäfer M, Baumeister T. Prosthetic fitting following amputations on the foot. Vol. 17, *Fuss und Sprunggelenk.* 2019. <https://doi.org/10.1016/j.fuspru.2019.07.003>
26. Seel T, Raisch J, Schauer T. IMU-based joint angle measurement for gait analysis. *Sensors (Switzerland).* 2014 Apr 16;14(4):6891–909.

<https://doi.org/10.3390/s140406891>

27. Shepherd MK, Gunz D, Clites T, Lecomte C, Rouse EJ. Designing Custom Mechanics in Running-Specific Prosthetic Feet via Shape Optimization. *IEEE Trans Biomed Eng.* 2023;70(2). <https://doi.org/10.1109/TBME.2022.3202153>
28. Siddiqui MIH, Arifudin L, Alnaser IA, Alluhydan K. Numerical Investigation on the Performance of Prosthetic Running Blades by Using Different Materials. *Journal of Disability Research.* 2023;2(1):6–13. <https://doi.org/10.57197/JDR-2023-0001>
29. Singh Sidhu HJ, Kumar S. Design and Fabrication of Prosthetic Leg. *a Journal of Composition Theory.* 2019;XII(VII).
30. Sundararaj S, Subramaniyan G v. Structural design and economic analysis of prosthetic leg for below and above knee amputation. *Mater Today Proc [Internet].* 2020;37(Part 2):3450–60. Available from: <https://doi.org/10.1016/j.matpr.2020.09.331>
31. Tabucol J, Brugo TM, Povolo M, Leopaldi M, Oddsson M, Carloni R, et al. Structural fea-based design and functionality verification methodology of energy-storing-and-releasing prosthetic feet. *Applied Sciences (Switzerland).* 2022;12(1). <https://doi.org/10.3390/app12010097>
32. Talla HK, Oleiwi JK, Hassan AKF. Performance of athletic prosthetic feet made of various composite materials with pmma matrix: numerical and theoretical study. *Revue des Composites et des Materiaux Avances.* 2021;31(4):257–64. <https://doi.org/10.18280/rcma.310410>
33. Yang X, Zhao R, Solav D, Yang X, Lee DRC, Sparrman B, et al. Material, design, and fabrication of custom prosthetic liners for lower-extremity amputees: A review. *Med Nov Technol Devices.* 2023;17. <https://doi.org/10.1016/j.medntd.2022.100197>
34. Yasser A. Design and Structural Analysis of Composite Prosthetic Running Blades for Athletes: A case of dynamic explicit analysis using Abaqus CAE. 2020;(June). Available from: <https://www.researchgate.net/publication/342336561Design> and Structural Analysis of Composite Prosthetic Running Blades for Athletes A case of dynamic explicit analysis using Abaqus CAE
35. Yusof KH, Zulkipli MA, Ahmad AS, Yusri MF, Al-Zubaidi S, Mohammed MN. Design and Development of Prosthetic Leg with a Mechanical System. In: 2021 IEEE 12th Control and System Graduate Research Colloquium, ICSGRC 2021 - Proceedings. 2021. <https://doi.org/10.1109/ICSGRC53186.2021.9515198>
36. Zadpoor AA, Asadi Nikooyan A, Reza Arshi A. A model-based parametric study of impact force during running. *J Biomech.* 2007;40(9). <https://doi.org/10.1016/j.jbiomech.2006.09.016>
37. Zhang T, Bai X, Liu F, Fan Y. Effect of prosthetic alignment on gait and biomechanical loading in individuals with transfemoral amputation: A preliminary study. *Gait Posture.* 2019 Jun 1;71:219–26. <https://doi.org/10.1016/j.gaitpost.2019.04.026>